frontiers in Energy Research

ORIGINAL RESEARCH
published: 04 May 2021
doi: 10.3389/fenrg.2021.640664

Comparative Investigation of Fullerene $PC_{71}BM$ and Non-fullerene ITIC-Th Acceptors Blended With P3HT or PBDB-T Donor Polymers for PV Applications

Francis Otieno[1,2], Lesias Kotane[2], Mildred Airo[1,3], Rudolph M. Erasmus[2], Caren Billing[1], Daniel Wamwangi[2] and David G. Billing[1]*

[1] Molecular Science Institute, School of Chemistry, University of the Witwatersrand, Johannesburg, South Africa, [2] Material Physics Research Institute, School of Physics, University of the Witwatersrand, Johannesburg, South Africa, [3] Institute for Nanotechnology and Water Sustainability, University of South Africa, Johannesburg, South Africa

OPEN ACCESS

Edited by:
Tayebeh Ameri, Ludwig Maximilian University of Munich, Germany

Reviewed by:
Safa Shoaee, University of Potsdam, Germany
Derya Baran, King Abdullah University of Science and Technology, Saudi Arabia
Ergang Wang, Chalmers University of Technology, Sweden

***Correspondence:**
Francis Otieno
frankotienoo@gmail.com

Specialty section:
This article was submitted to Solar Energy, a section of the journal Frontiers in Energy Research

Received: *11 December 2020*
Accepted: *31 March 2021*
Published: *04 May 2021*

Citation:
Otieno F, Kotane L, Airo M, Erasmus RM, Billing C, Wamwangi D and Billing DG (2021) Comparative Investigation of Fullerene $PC_{71}BM$ and Non-fullerene ITIC-Th Acceptors Blended With P3HT or PBDB-T Donor Polymers for PV Applications. Front. Energy Res. 9:640664. doi: 10.3389/fenrg.2021.640664

Fundamentally, organic solar cells (OSCs) with a bulk-heterojunction active layer are made of at least two electronically dissimilar molecules, in which photoabsorption in one (donor) generates Frenkel excitons. The formation of free charge carriers emerge after exciton dissociation at the donor:acceptor interface. In the past decade, most of the progress in enhanced device performance has been steered by the rapid development of novel donor and acceptor materials and on device engineering. Among these donor materials, regioregular poly(3-hexylthiophene) (P3HT) produced better performance despite the mismatch of its absorption coefficient with the solar emission spectrum. Comparatively the donor PBDB-T exhibits an outstanding absorption coefficient with a deeper-lying highest occupied molecular orbital (HOMO) level. Previously most of the efficient acceptors were based on fullerene molecules characterized by limited photoabsorption and stability. In contrast, the recently developed non-fullerene OSCs have a tunable absorption spectrum and exhibit improved stability. In this work, we explore the fundamental sources of the differences in the device performance for different blend compositions made of fullerene derivative ($PC_{71}BM$) and non-fullerene (ITIC-Th) when paired with the polymer donors P3HT and PBDB-T. The characteristic changes of the optical properties of these blends and their roles in device performance are also investigated. We also studied charge generation where PBDB-T:$PC_{71}BM$ showed the highest maximum exciton generation rate (G_{max}) of 3.22×10^{28} s^{-1} while P3HT: ITIC-Th gave the lowest (0.96×10^{28} s^{-1}). Also noted, $PC_{71}BM$ based counterparts gave better charge transfer capabilities as seen from the lower PL quenching and higher charge carrier dissociation plus collection probability P(E,T) derived from a plot of J_{ph}/J_{sat} ratio under short-circuit conditions against the effective voltages.

Keywords: absorption, charge generation and recombination, bulk-heterojuction, Photoluminesce property, Raman spcctroscopy

INTRODUCTION

In the past decade, bulk heterojunction (BHJ) organic solar cells (OSCs) have been intensively studied for their high potential for realizing environmentally friendly, low cost, non-complex, and flexible large area devices (Zhou et al., 2012; Liu et al., 2015). Despite the rapid improvement in the power conversion efficiency in the recent past, the progress toward commercialization of these devices is still hindered by their low carrier mobility, insufficient photoabsorption (Li et al., 2018), and degradation by intrinsic factors such as inter-layer molecular cross diffusion. Additionally, external factors such as moisture and photo-oxidation have been found to affect device stability (Zakhidov et al., 2020). One strategy to enhance the device performance is to increase the photo generated current through extending the light harvesting capabilities to a broad absorption window (Yang et al., 2019). This has seen the development of numerous donor and acceptor materials with varied band gaps as well as the design of many classical donor/acceptor heterojunction systems (Gao et al., 2017).

Among the most investigated donor material is regioregular poly(3-hexylthiophene) (P3HT) known for extremely important structural and photophysical properties leading to devices with high PCE (Zhang et al., 2019). This is attributed mainly to self-organization of its molecules as laminar structures with crystal properties that enable high hole mobility ($>10^{-2}$ cm^2/Vs) (Qin et al., 2016). However, PH3T is also known to have a mismatched absorption spectrum in relation to the solar emission spectrum which confines photoabsorption to wavelengths below 650 nm (Kroon et al., 2008; Smestad et al., 2008). This mismatch is associated with transmission losses that need to be circumvented for enhanced functionality. One approach toward increasing the degree of absorption matching involves the evolution of novel donor polymers. Hence Poly[(2,6-(4,8-bis(5-(2-ethylhexyl)thiophen-2-yl)-benzo[1,2-b:4,5-b']dithiophene))-alt-(5,5-(1',3'-di-2-thienyl-5',7'-bis(2-ethylhexyl)benzo[1',2'-c:4',5'-c']dithiophene-4,8-dione)], PBDB-T has gained widespread attention as an alternative donor component of the bulk heterojunction. Bulk heterojunctions with PBDB-T blend have registered high efficiencies of up to 12% (Li et al., 2016; Zhao et al., 2017) and this has been attributed to its extended absorption coefficient, high charge carrier mobility, moderate band gap and a deep-lying highest occupied molecular orbital (HOMO) level (Qian et al., 2012). This HOMO level is essential for the realization of larger values of the open circuit voltage. Besides excellent optical properties, morphology plays a prominent role in the charge extraction and transport. Thus its complementary absorption spectra and aggregation properties create a favorable morphology for high exciton generation rate and charge transport (Gurney et al., 2019). The choice of the acceptor molecule is another crucial factor to consider in order to realize the desired high power conversion efficiencies.

The past decades have experienced a surge in the use of fullerene derivatives such as $PC_{61}BM$ and $PC_{71}BM$ (Falke et al., 2014; Zhao W. et al., 2015; Otieno et al., 2016, 2017) as electron acceptors due to their favorable electron affinity. These ball-like fully conjugated structures have strong electron affinity and unipolar electron transport that promotes delocalization of electrons (Gélinas et al., 2014). Nevertheless, these fullerene derivatives have been characterized by a relatively narrow absorption band within the visible spectrum range and high production cost owing to their processing steps that require purification (Zhao J. et al., 2015). Thus, the search for better electron acceptor materials continues to steer intensive research into alternative OSCs. This forms the basis for the rapidly emerging popularity of non-fullerene acceptors (NFA) which are small polymer molecules famous for their smaller bandgap (Lin and Zhan, 2014; San Juan et al., 2016). The broad array of the NFA landscape has shown their versatility in the tuning of their opto-electrical properties through molecular design. Thus large values of V_{oc} can be realized by matching their energy levels with other electron donating polymers (Liu et al., 2016). 3,9-Bis(2-methylene-(3-(1,1-dicyanomethylene)-indanone))-5,5,11,11-tetrakis(5-hexylthienyl)-dithieno[2,3-d:2',3'-d']-s-indaceno[1,2-b:5,6-b'] dithiophene (ITIC-Th) is among the most popular non-fullerene known for good performance as a result of its deeper molecular orbitals (HOMO = −5.66 eV, LUMO = −3.93 eV), that matches most high-performance varied band-gap polymer donors (Lin et al., 2016). The structures of these donor and acceptor materials are shown in **Figure 1**.

In this study, our aim is to directly compare the physical properties of pristine donor and acceptor materials and their role in the overall properties of the photoactive layer upon formation of binary blends based on two contrasting acceptors ($PC_{71}BM$ and ITIC-Th) and two donor polymers (PBDB-T and P3HT). We probe the photovoltaic performance of the four BHJ blends looking into the device physics and structure to establish the origins of the variation in performance. Steady-state absorption and emission spectroscopy are used to study charge generation, separation, and recombination in the devices.

EXPERIMENTAL PROCEDURE

Materials and Procedure

Indium tin oxide (ITO) glass (surface resistivity: 30–60 Ω/sq.), P3HT and $PC_{71}BM$ were bought from Sigma-Aldrich. The ITO glass was cut, then cleaned and dried using the procedure described elsewhere (Otieno et al., 2016). PEDOT:PSS (1.3 wt% dispersion in H_2O), PBDB-T-SF (PCE13) and ITIC-Th, were sourced from Ossila Limited. The donor:acceptor blends were mixed in a ratio of 1:1 to form a 20 mg/ml solution and then stirred overnight to ensure a homogeneous blend solution. The sequential device fabrication was carried out foremost by spin coating PEDOT:PSS onto etched ITO glass substrates. The PEDOT:PSS layers were further annealed at 100°C for 10 min to remove water residue before spin coating the blend mixture on the PEDOT:PSS/ITO layers. The photoactive layer comprising of the polymer blend was spin coated at 2,000 rpm for 1 min. The donor:acceptor/PEDOT:PSS/ITO layers on glass were metallized by thermal evaporation of Al to form the ITO/PEDOT:PSS/binary blend/Al device architecture. The resulting OPV device was annealed over a hot plate for 10 min

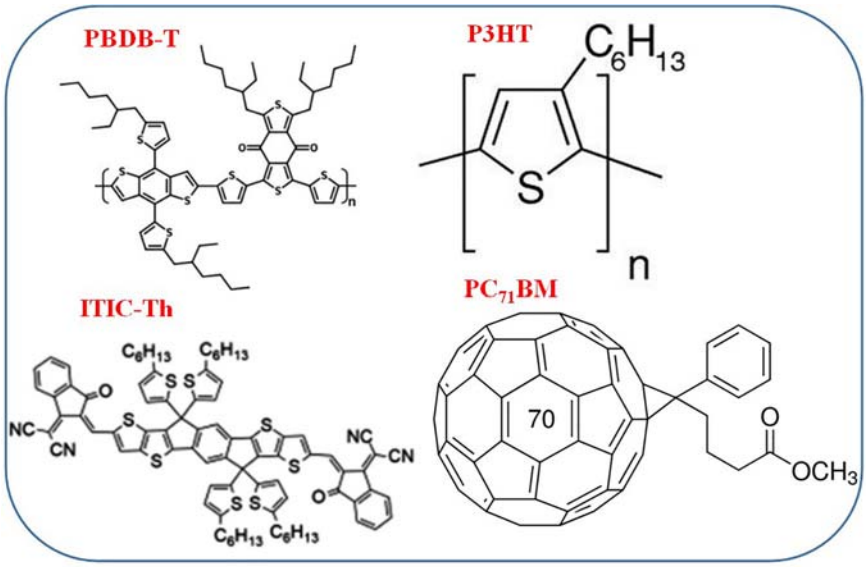

FIGURE 1 | Chemical structure of donor materials PBDB-T, P3HT, and acceptor ITIC-Th and $PC_{71}BM$.

at 120°C to increase the interconnectivity of the blend network (Otieno et al., 2017).

Characterization Techniques

A Cary 500 UV–Vis-NIR Spectrophotometer was used to measure the optical absorption of the thin films. Both Photoluminescence and Raman spectra were measured using a Horiba LabRAM HR Raman spectrometer with 600 lines/mm grating using a 514.5 nm excitation wavelength from an argon-ion laser. A laser power of 4 μW at the sample was used to prevent laser damage to the thin film. Current density–voltage (*J–V*) characteristics were measured using a solar simulator (fitted with 150 W Xe lamp) with 1.5 air mass filters and a (HP 4141B DC) source/measure unit under 100 mW/cm^2 illumination. It is crucial to note that all devices were prepared and characterized in air prompting the slight lower *J–V* performances witnessed. The thicknesses of the PEDOT:PSS layer, the active layer of various blends and the Al electrode were measured to be about 50, 215, and 300 nm with negligible variations, respectively using a surface profilometer. Over 10 devices were fabricated and characterized for each active layer combination and a standard deviation calculated.

RESULTS AND DISCUSSION

UV–Vis Spectroscopy

The absorption spectrum of each individual layer prior to blend formation is presented in **Supplementary Figure 1**. It is seen in the figure that PBDB-T has strong absorption in the range spanning from 500 to 750 nm. Additionally, a less intense absorption peak is evident in the ultraviolet range around 350 nm. The extent of the absorption window within the visible range is much broader for this donor material compared to that of P3HT ($550 < \lambda < 650$ nm) thus highlighting the superior spectral broadening characteristics of PBDB-T. This comparison was extended to the two contrasting individual acceptor layers. **Supplementary Figure 1** shows that the non-fullerene derivative ITIC-Th has a very large extinction coefficient (k) and an extended absorption characterized by two peaks at ∼575 and 640 nm compared to the fullerene derivative counterpart $PC_{71}BM$ which peaks at ∼474 nm. Based on these results, thin films of the polymer blends of comparable film thickness were subsequently analyzed. The active layer thickness for all blends was approximately 215 nm.

It is evident that upon blend formation (see **Figure 2**), non-fullerene ITIC-Th based blends show broader and stronger

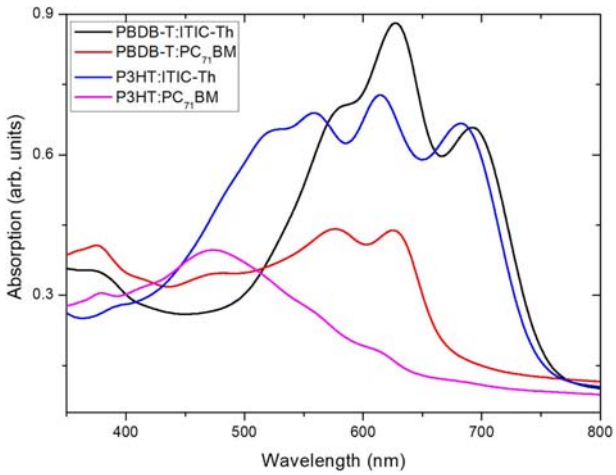

FIGURE 2 | Absorption spectra of different D:A thin films blends.

absorption compared to the fullerene, $PC_{71}BM$ based blends. Among the ITIC-Th based blends, the PBDB-T:ITIC-Th blend shows a higher absorption intensity although with a narrower wavelength range compared to P3HT:ITIC-Th. This implies that absorption beyond the bluish-green portion of the EM spectrum is reduced for the PBDB-T based blend layer. However, there is reasonable agreement that all the ITIC-Th based blends have a better light harvesting capability compared to $PC_{71}BM$ based counterparts for the same film thicknesses.

Photoluminescence Spectroscopy

Supplementary Figure 2 shows the steady-state photoluminescence measurements of pristine PBDB-T, P3HT, ITIC-Th, and $PC_{71}BM$ thin films spin coated as single layers on glass substrates. These measurements have been carried using the 514.5 nm laser line as the excitation wavelength. All the films emit in the visible and near infrared range. The normalized PL spectrum (blue line) of **Supplementary Figures 3, 4** show a stronger overlap of the emission of PBDB-T and P3HT, respectively, with the absorption of non-fullerene ITIC-Th compared to the fullerene counterparts. This overlap is likely to assist in the energy transfer from the donor to the ITIC-Th via Forster resonance energy transfer (FRET) thus leading to localized absorption. The quenching of the PL emission upon blend formation suggests possible energy transfer between the donor and acceptor material. **Figure 3** shows higher PL quenching from the fullerene acceptor-based blends as compared to their non-fullerene counterpart and this is an indication of a more favorable change transfer mechanism than the energy transfer mechanism. The efficiency of the charge transfer is usually dependent on the mean length between conjugated polymer donor and fullerene/NFA molecules. The high PL emission (low PL quenching) experienced with the NFA blends indicates that the donor - non-fullerene interface may exceed the exciton diffusion length (˜10 nm). Hence it is also plausible that some excitons cannot rapidly dissociate as the nearest NFA molecule is much further than the exciton diffusion length. The consequence of this is a radiative recombination that gives rise to the intense photoluminescence signal (Motaung et al., 2009) seen in **Figure 3**. Since the radiative recombination leads to the loss of charge carriers and thus to a reduction in the photocurrent, re-absorption of the radiated photon by the donor cannot be ruled out. Comparing the donor materials for the same acceptor, PBDB-T: PC71BM show better PL quenching, an indication of better charge transfer compared to P3HT: PC71BM. This is in agreement with the difference in *J–V* performance in section "*J–V* Characterization Under Illumination." On the contrary, P3HT:ITIC-Th showed higher PL quenching compared to PBDB-T:ITIC-Th despite poor device performance in section "*J–V* Characterization Under Illumination." This high unusual PL quenching in P3HT:ITIC-Th compared to PBDB-T:ITIC-Th could be attributed to either additive photo-absorption in the acceptor and donor leading to the generation of more electrons besides that of the donor or due to photoexcitation of the donor by the emission from the ITIC-Th.

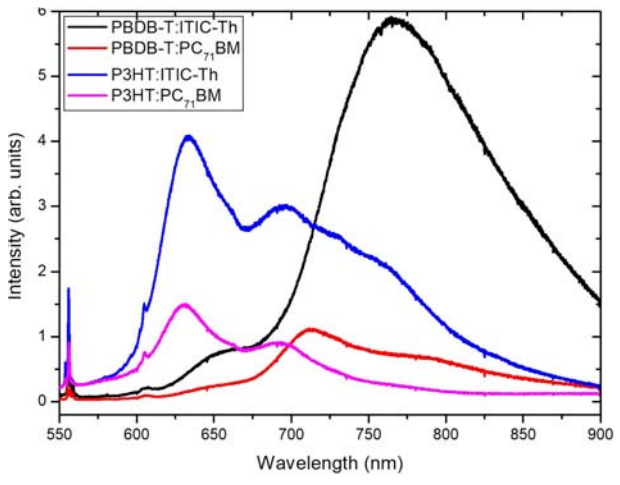

FIGURE 3 | PL spectra of different D:A thin films blends.

Raman Spectroscopy

When organic molecules experience electronic transitions induced by light, new forces in the excited state within their nuclear framework occurs such that atoms are displaced from their ground state equilibrium positions. Such motions can be ascribed to Raman-active vibrations (i.e., totally symmetric vibrations) hence ensuring a metastable configuration of the Franck-Condon geometry (Grey, 2019).

Usually, electronic transitions of conjugated polymer materials are mostly π-π^* in nature. This means higher frequency skeletal C–C stretching modes in the range of 1,000–1,600 cm^{-1} as depicted in **Figure 4**. This figure shows the Raman spectra of different blends while the in-set is a magnified view of the spectra between 1,350 and 1,550 cm^{-1}. From **Supplementary Figure 3**, PBDB-T shows more polymer crystallization from the sharp Raman peaks compared to P3HT donor material ensuring enhanced regioregular domains (Kim et al., 2011; Roigé et al., 2012). Such increased degree of crystallinity is known to induce a larger interchainmolecular interaction leading to more delocalized conjugated π electrons, consequently producing a low band gap and enhanced optical π–π^* transition resulting in a more effective photon absorption (Motaung et al., 2009) as depicted in **Figure 2**. Pristine PBDB-T used as a donor shows Raman modes at 1,427, 1,452, 1,487, and 1,540 cm^{-1}, which are assigned to the C_α=C_β symmetric stretching mode, antisymmetric stretch mode of C_α=C_β, skeletal stretching mode of C_β–C_β and antisymmetric C_α–S–C_α ring skeleton that depict distortion of the in-plane vibrations of the thiophene ring of PBDB-T (Gao et al., 2018). Other less intense peaks are at 1,075, 1,231, and 1,598 cm^{-1} and may be assigned to the stretching mode of C_β–C_{alkyl}, C–H bending mode, and antisymmetric stretch mode of C_α=C_β, respectively (Kabongo et al., 2016). Upon blending with acceptor materials, there is no noticeable shift in peak position regardless of whether ITIC-Th (non-fullerene) nor $PC_{71}BM$ (fullerene) is used. This indicates that the two acceptor materials are being loaded onto the PBDB-T polymer backbone without much alteration of the conjugation

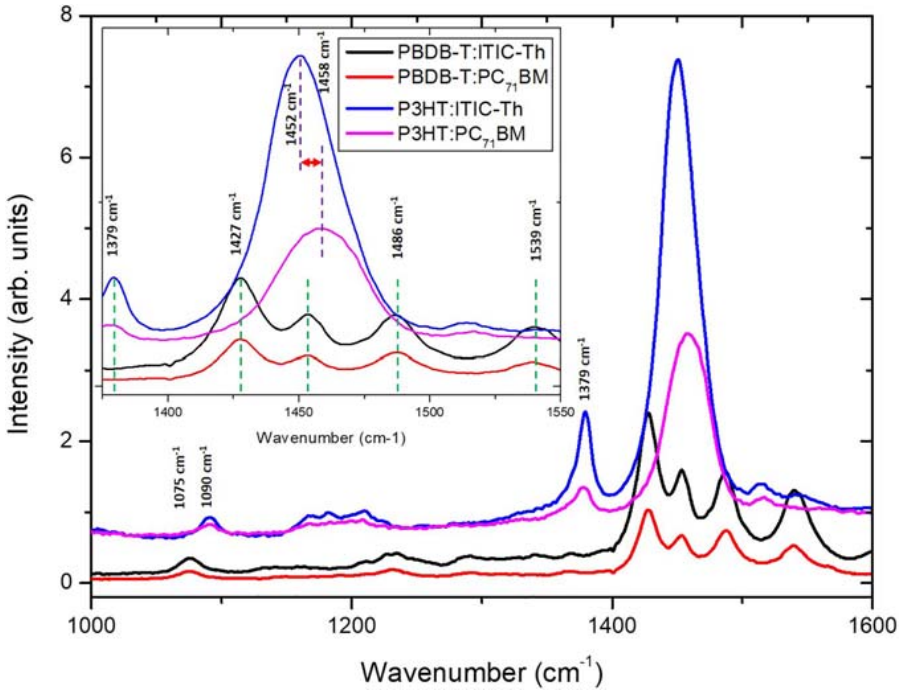

FIGURE 4 | Comparison of Raman spectra for thin films of various D:A blends.

length of the polymer (Falke et al., 2011). However, there is a general increase in intensity upon blending with PBDB-T, an indication of a preresonant Raman effect as a result of some absorption around the 514 nm excitation wavelength within the blend films (Tsoi et al., 2011).

The P3HT donor shows three main peaks at 1,090, 1,379, and 1,450 cm^{-1} that can be assigned to the C–H bending mode, the C_β–C_β skeletal stretch mode, and the C_α=C_β symmetric stretch mode, respectively (Falke et al., 2011), as shown in **Supplementary Figure 3**. The most prominent band of the pristine P3HT is at 1,450 cm^{-1} with a FWHM of 27.63 cm^{-1}. Upon blending with ITIC-Th, the only significant change was a FWHM increased to 37.03 cm^{-1}. Blending P3HT with $PC_{71}BM$ acceptor material, the prominent peak shifted to 1,458 cm^{-1} while FWHM increased further to 40.03 cm^{-1}. This difference between the polymer/fullerene blend signals is shown in the inset (**Figure 4**). The shift to a higher wavenumber indicates a further shrinking of the conjugation length along the polymer backbone and increased FWHM indicates a crystallinity decrease of the P3HT polymer. This shift is more pronounced for the P3HT:$PC_{71}BM$ blend compared to the P3HT:ITIC-Th blend and this corroborates the difference in device performance experienced. On the other hand, P3HT:ITIC-Th shows a more intense peak at 1,452 cm^{-1} compared to P3HT:$PC_{71}BM$, an indication of a more ordered structure leading to an increase of the Raman cross-section (Roigé et al., 2012). Such enhanced intensity characteristics are induced by morphological changes associated with polymer crystallization transitions leading to large phase separation that is likely to affect charge transfer as observed in the *J-V* characteristics.

J–V Characterization in the Dark

For a *J–V* graph measured in the absence of light, the dark current can be categorized into three sections corresponding to various types of charge transport within the device depicted by the semi-logarithmic representation in **Figure 5**.

In region (i), located mainly below the open circuit voltage of the OPVs (0–0.5 V), the current is mainly being limited by shunt resistance Rsh. The charge carrier injection emanating from the electrodes into the polymer material is usually minimal as a result of the low bias voltage unable to compensate for the internally built-in field (Gadisa, 2006). In this region, P3HT:ITIC-Th shows the highest current which is attributed to the presence of shunt paths for the charge carriers resulting from the poor organization of the two polymers in the blend which lacks phase separation. PBDB-T:$PC_{71}BM$ blends on the other hand show the lowest dark current density in region (i) prompting decreased reverse dark saturation current density leading to enhanced V_{OC} of the devices as defined by: $Voc = \frac{nkT}{q}(\ln \frac{J_{ph}}{J_s} + 1)$ (He et al., 2010), where n is the ideality factor, k is the Boltzmann constant, q is the elementary charge, T is the temperature in kelvin, J_{ph} is the photocurrent and J_S is the reverse dark saturation current density. In region (ii), the current is controlled by the diode characteristics; bias saturation current density J_0 and ideality factor n, usually factors attributed to the metal-active layer interface of the device (Servaites et al., 2011). The four devices show almost the same slope in this region and thus similar diode characteristics. Generally, the same donor materials exhibit similar dark current behavior at 1.0 V [region (iii)], an indication of similar carrier mobilities in the blends. Region (iii) is associated

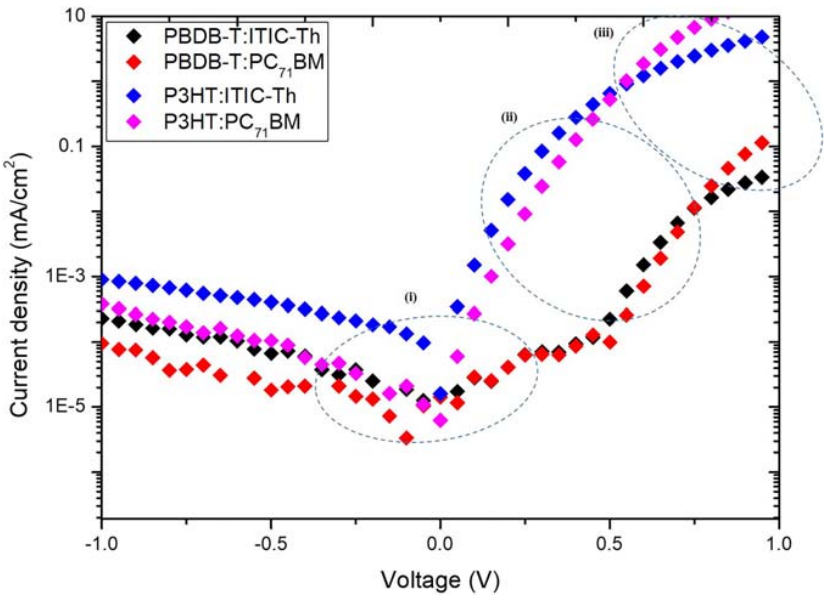

FIGURE 5 | Semi-logarithmic current density vs. voltage characteristics of various blends.

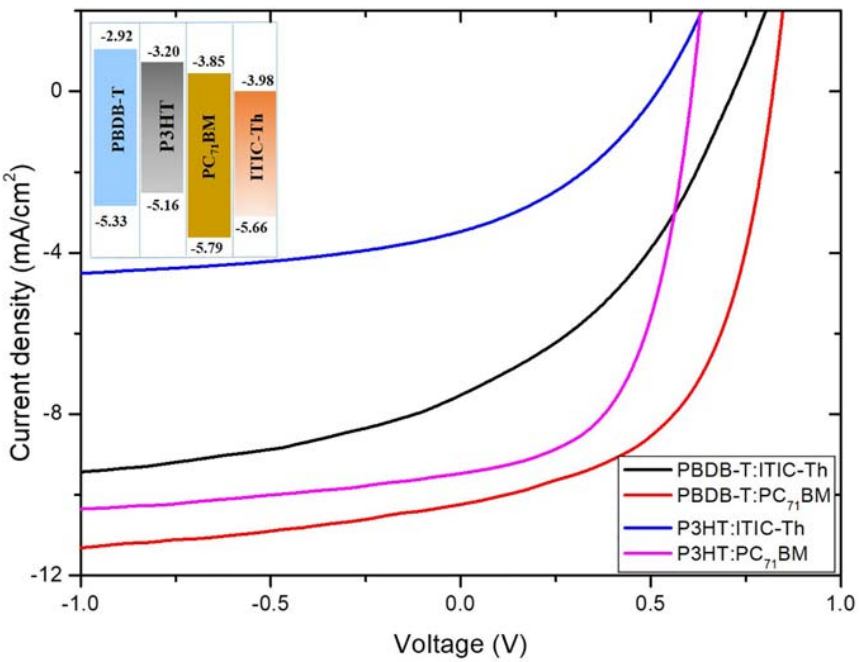

FIGURE 6 | The current density–voltage (*J–V*) characteristics of devices with various blend ratios under simulated air mass (AM 1.5) irradiation (100 mW/cm^2), inset is energy level orbitals of polymers.

with charge transport in the bulk/blend material and corresponds to space charge limited region. Organic polymer blends have low charge carrier mobility due to the presence of traps, impurities and series resistance (Rs) limited currents, thus the transfer rate of injected charge carriers is highly diminished resulting in charge accumulation in most active organic materials (Martens et al., 2000). A steep slope in this region similar to the PBDB-T:$PC_{71}BM$ blend imply high Rs in the device that aid in better charge collection at the electrodes.

J–V Characterization Under Illumination

Figure 6 shows the current density–voltage (*J–V*) characteristics of various OPV devices measured under AM 1.5 G illumination with 100 mW/cm^2 light intensity. The inset shows the energy

TABLE 1 | Performance characteristics of different devices.

Device	Voc (V)	Jsc (mA/cm^2)	Rs (Ω)	Rsh (kΩ)	FF (%)	PCE (%)
PBDB-T:ITIC-Th	0.71 ± 0.12	7.47 ± 0.15	57.4 ± 1.2	191 ± 3	37.6 ± 1.1	2.0 ± 0.2
PBDB-T:$PC_{71}BM$	0.82 ± 0.14	10.22 ± 0.10	85.3 ± 2.3	161 ± 2	53.5 ± 1.1	4.5 ± 0.4
P3HT:ITIC-Th	0.51 ± 0.10	2.29 ± 0.18	212.9 ± 1.5	209 ± 5	34.2 ± 1.1	0.6 ± 0.1
P3HT: $PC_{71}BM$	0.60 ± 0.12	9.45 ± 0.12	34.4 ± 0.9	267 ± 2	54.2 ± 1.2	3.1 ± 0.2

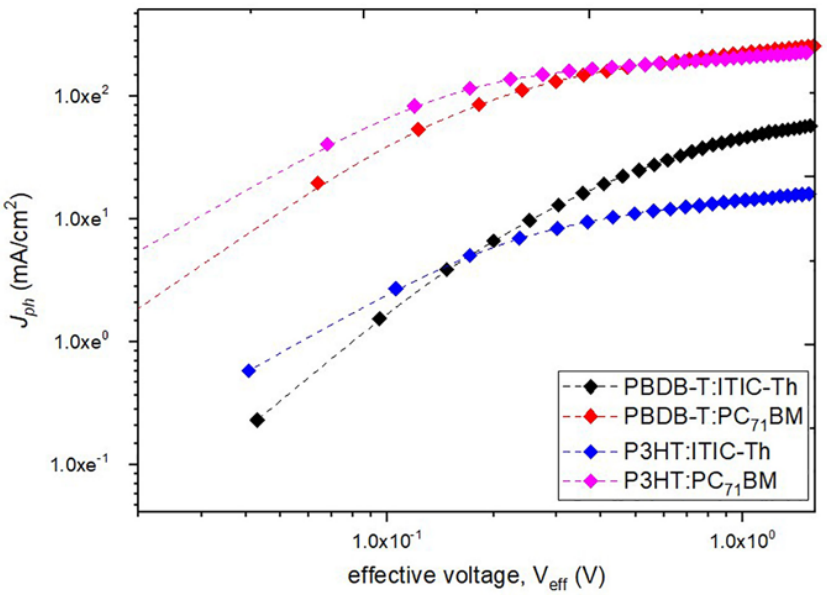

FIGURE 7 | Photocurrent density versus effective voltage curves of solar cells based on different blends.

level orbitals of the polymers while **Table 1** gives the extracted device characteristics.

Based on their favorable energy-level alignment as depicted in the inset of **Figure 6**, all these donor/acceptor combinations demonstrate a high possibility of achieving efficient charge separation. P3HT:ITIC-Th recorded the lowest performance with fill factor (FF) of 34.2%, J_{sc} of 2.29 mA/cm^2 and V_{oc} of 0.51 V resulting in a PCE of 0.61%. Such low Voc is as a result of the small HOMO-LUMO difference of the donor-acceptor compared to other blends since the Voc of OPVs is directly proportional to the difference in energies of the LUMO and HOMO of the acceptor and the donor, respectively (Qin et al., 2016). Generally, P3HT has an ionization potential of ∼–5.16 eV hence devices in which it is used as a donor material experienced lower Voc compared to their PBDB-T counterparts with ionization potential of ∼–5.33 eV. When the donor material was PBDB-T, a blend of PBDB-T:$PC_{71}BM$ gave a greater V_{oc} of 0.82 V in comparison to PBDB-T:ITIC-Th that gave 0.71 V. This could be attributed to a higher-lying LUMO level (–3.85 eV) compared to that of ITIC-Th (-3.98 eV).

PBDB-T:$PC_{71}BM$ recorded the highest short circuit current density of 10.22 mA/cm^2 with a fill factor of 53.5% yielding best conversion efficiency of 4.5%. This high current could be attributed to a better charge transfer as witnessed from the high PL quenching discussed in section "Raman Spectroscopy" despite the low absorption intensity compared to other blends. P3HT:$PC_{71}BM$ was second best in terms of current density among the four blends. This finding is also attributed to better charge transfer at the donor-acceptor boundaries.

Charge Generation and Dissociation Dynamics

We further carried out studies on charge generation and separation. **Figure 7** shows a plot of photocurrent density J_{ph} against the effective voltage V_{eff} where J_{ph} is defined as $J_{ph} = J_L - J_d$. J_L and J_d stand for the current densities under illumination and in the dark, respectively. The effective voltage V_{eff} was defined as V_0 - V, where V_0 is the voltage at which $J_L = J_d$.

From **Figure 7**, the photocurrent is linearly proportional to the voltage at low effective voltages (V_{eff} < ∼0.1) and thereafter saturates at higher V_{eff} (>1) where minimal charge recombination is expected as a result of the high internal electric field within the device (Xiao et al., 2018). From this graph, the saturation photocurrent density (J_{sat}), which is usually only limited by the incident photon flux absorbed by the active layer and is independent of the temperature and bias voltage (Chen et al., 2015), can be calculated and the results are shown in **Table 2**. PBDB-T:$PC_{71}BM$ experiences a high saturation current (11.08 mA/cm^2), an indication of better charge

TABLE 2 | Derived saturation photocurrent density, maximum exciton generation rate and charge dissociation and collection probability.

Device	J_{sat} (mA/cm^2)	G_{max} ($s^{-1} \times 10^{28}$)	P(E,T) (%)
PBDB-T:ITIC-Th	5.73 ± 0.15	1.67 ± 0.05	70.9 ± 0.5
PBDB-T:$PC_{71}BM$	11.08 ± 0.12	3.22 ± 0.11	85. 4 ± 0.4
P3HT:ITIC-Th	3.32 ± 0.10	0.96 ± 0.10	66.2 ± 0.1
P3HT: $PC_{71}BM$	10.52 ± 0.05	3.05 ± 0.12	90.6 ± 0.2

carrier transmission and collection compared to P3HT:ITIC-Th (3.32 mA/cm^2). From the derived saturation current, we can derive the maximum exciton generation rate (G_{max}) which is an indication of the maximum number of absorbed photons, and is given by $J_{sat} = qL\ G_{max}$, where q is the basic charge and L is the photoactive layer thickness, about 215 nm (Lu et al., 2015). PBDB-T:$PC_{71}BM$ showed the highest maximum exciton generation rate (G_{max}) of 3.22×10^{28} s^{-1} followed by P3HT:$PC_{71}BM$ (3.05×10^{28} s^{-1}), an indication that binary blends of fullerene derivative $PC_{71}BM$ have high light absorption and harvesting contrary to the UV-vis spectra (with low absorption intensity but broader range) leading to the high J_{sc} for the devices. This illustrates that absorption within a wider range of the solar spectrum is quite crucial in ensuring more light harvesting by the solar cell devices.

Charge dissociation and collection probability P(E,T) of different devices was thereafter analyzed using a plot of the J_{ph}/J_{sat} ratio under short-circuit conditions against the effective voltages (Qin et al., 2016) as shown in **Figure 8**. The P3HT:$PC_{71}BM$ blend showed the highest value of P(E,T) of 90.62% which is correlated with the highest fill factor of 54.2% recorded in section "Raman Spectroscopy" while P3HT:ITIC-Th gave the lowest value leading to lowest PCE. This indicates that when $PC_{71}BM$ is used as an acceptor material, lower geminate recombination at the donor–acceptor interface is experienced as indicated by the higher charge dissociation probability compared to ITIC-Th counterparts resulting in more efficient charge generation processes hence higher current density.

Charge Recombination Dynamics

As shown in **Figure 9**, all four devices fabricated and tested showed a linear dependence of current density on light intensity in logarithmic coordinates, but with slightly different slopes. The current density J_{sc} is known to depend on the light intensity (P_{light}) through a power-law expressed as $Jsc \propto (P_{light})^{\alpha}$, for organic photovoltaics devices (Riedel et al., 2004), where α is the gradient of the log-log plot of Jsc against light intensity.

Usually an α value close to one gives an indication of a weaker bimolecular recombination under short circuit conditions. P3HT:$PC_{71}BM$ gave a slope of 0.978, close to the value of 0.971 of PBDB-T:$PC_{71}BM$. These high values close to 1 indicate that $PC_{71}BM$ based devices are much more capable of efficient sweeping out of charge carriers with negligible bimolecular recombination in comparison to their ITIC-Th counterparts. PBDB-T:ITIC-Th showed an α value of 0.797 while P3HT:ITIC-Th gave a value of 0.695. This indicates that the ITIC-Th based devices have increased bimolecular recombination that competes with charge extraction resulting in reduced current density recorded.

Figure 10 shows an investigation into the dominant recombination from Voc dependence on the natural logarithm

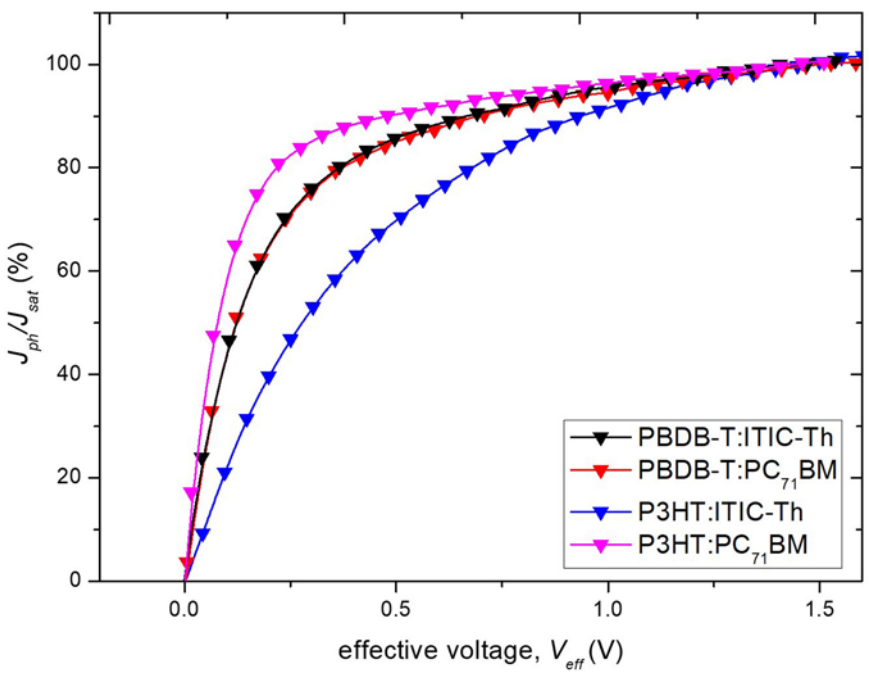

FIGURE 8 | P(E, T) against V_{eff}, where P(E, T) was derived using normalized J_{ph} with J_{sat} (i.e., J_{ph}/J_{sat}).

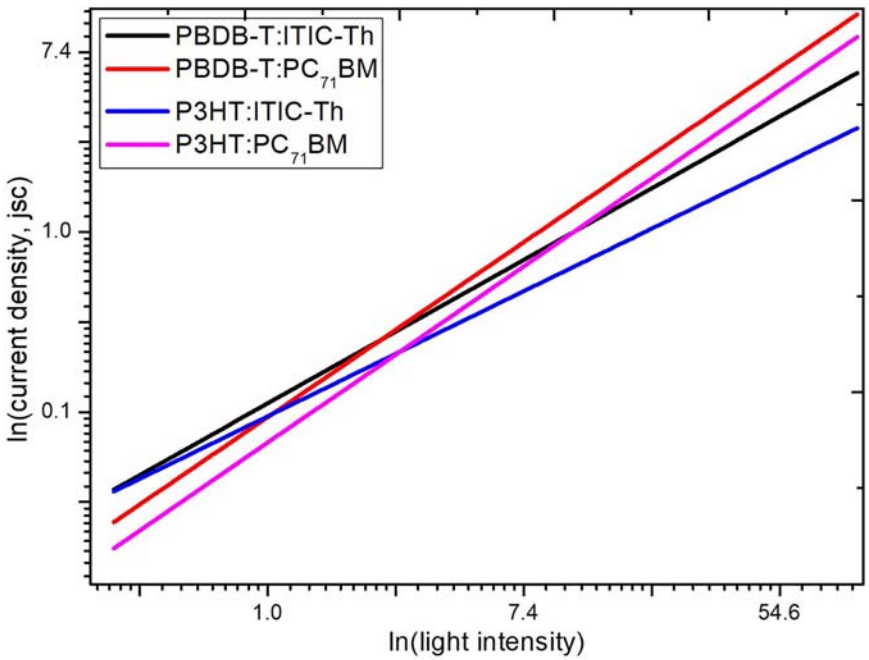

FIGURE 9 | Dependence of short-circuit current density on light intensity.

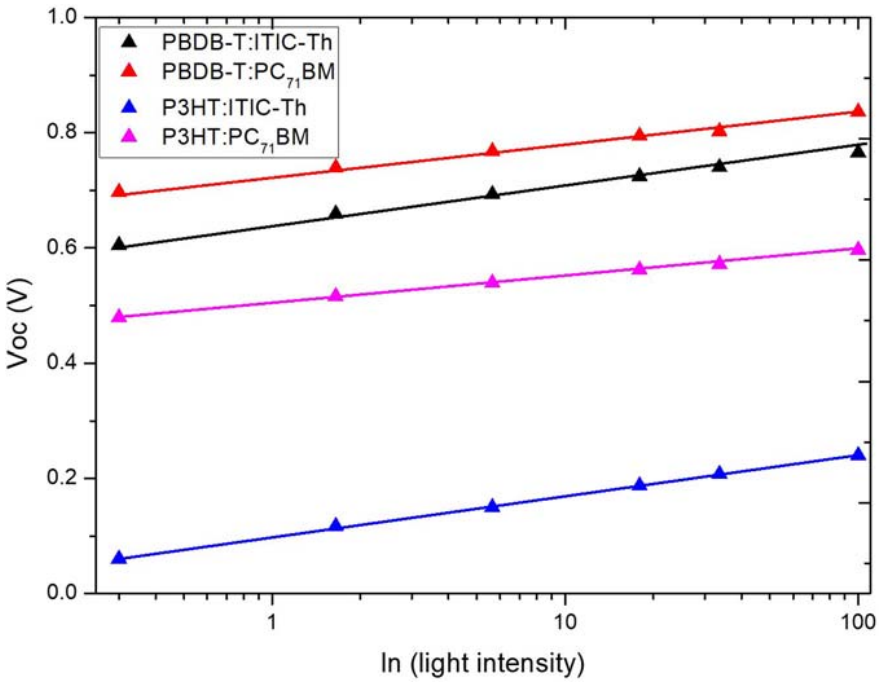

FIGURE 10 | Open-circuit voltage variation with Light intensity for various devices.

of varied intensity of light governed by the relationship Voc $\propto$ (nk$_B$T/q)log(P$_{light}$), where n represents the ideality factor, Boltzmann's constant is shown as k$_B$, T stand for temperature in Kelvin, and elementary charge is represented as q. The gradient of V_{oc} against ln(P$_{light}$) is shown to estimate the extent of trap-assisted recombination within the OPVs. P3HT:ITIC-Th reported the largest slope of 1.459 k$_B$T/q, an indication that the device experiences stronger trap-assisted or Shockley–Read–Hall recombination compared to other devices. On the other hand P3HT:PC$_{71}$BM showed the smallest

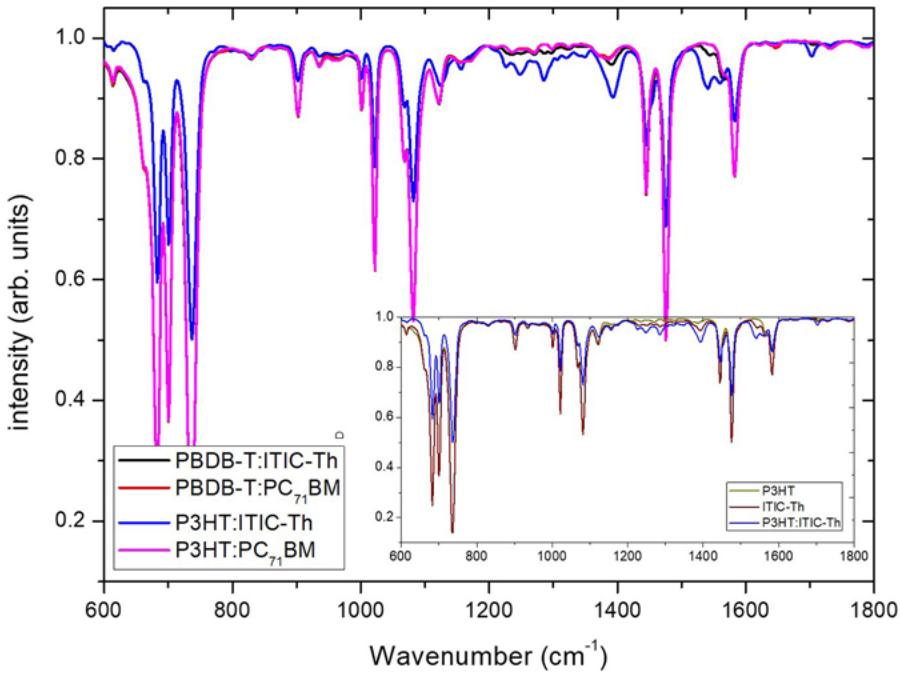

FIGURE 11 | FTIR spectra of various organic blends. Inset is a comparison of P3HT:ITIC-Th with the pristine components.

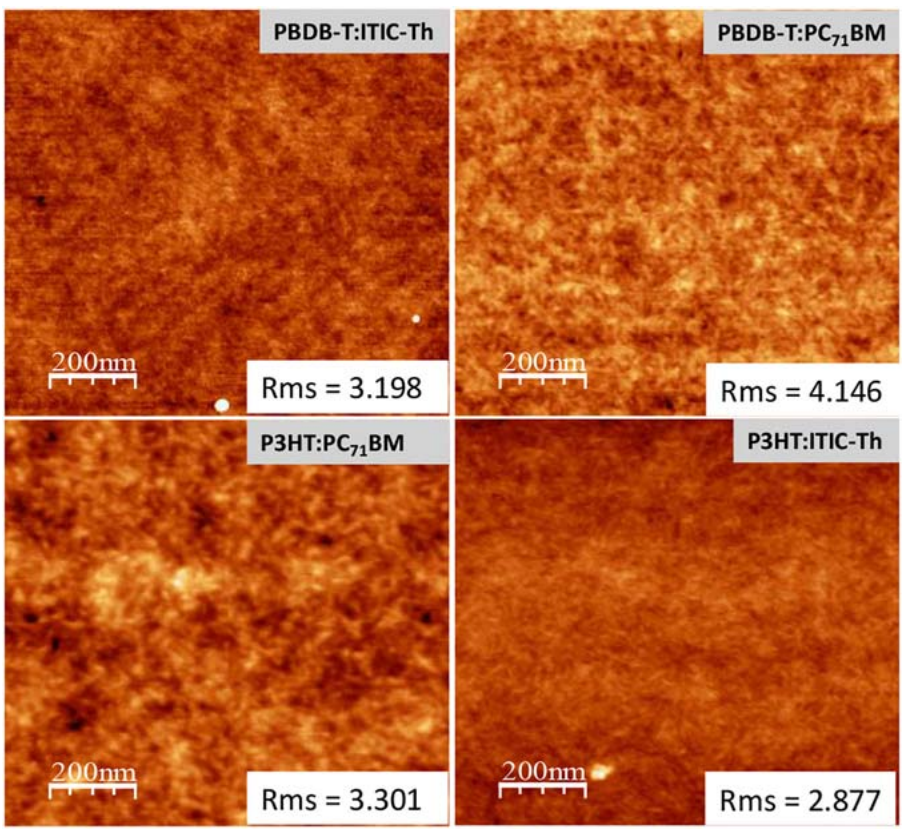

FIGURE 12 | Tapping mode AFM images measured for various thin film compositions.

slope of 0.975 k_BT/q indicating a dominance of bimolecular recombination mechanisms with fewer traps.

FTIR Measurements

The FTIR spectral characteristics of the pristine films and blends deposited on a glass substrate are shown in **Figure 11**. At wavenumber positions in the range of 650–1585 cm^{-1}, two clustered peaks can be observed which are attributed to the occurrence of C–H band symmetric and asymmetric vibrations (Arulraj et al., 2018).

From the spectra above, the pristine films showed similar peak positions with no significant shift upon blend formation. The peaks around 600–800 cm^{-1} are an indication of C–H bending vibrations out of the plane in which the thiophene ring vibrates while that at 903 cm^{-1} could be ascribed to C–H stretching vibrations. The peaks observed at 1,000–1,200 cm^{-1} are attributed to the COO- asymmetric and symmetric stretching vibrations of the surface acetate species (Suprunov and Ivanov, 1987), while those around 1,200–1,500 cm^{-1} are ascribed to C=C symmetric vibrations formation and that of 1,583 cm^{-1} is assigned to the C=C stretching mode (Nicho et al., 2004; Motaung et al., 2009). Upon blend formation, little or no shifts to either longer or shorter wavenumbers are seen; however, there is an increase in intensity of most vibrations, especially the aromatic-C–H out plane vibrations and aliphatic-C–H stretching. This suggests that blends differ in relative amount of twisting moiety in the crystalline state which appear highest in the P3HT:PC_{71}BM blend. This is in agreement with the highest value of P(E,T) of 90.62% reported and indicates better lamellae reorientation and high-mobility percolation paths formation with grain boundaries of low angle (Street et al., 2005). P3HT:ITIC-Th shows a great decrease in peak intensity when compared to its pristine components as shown in the inset in **Figure 10**. This explains the low performance of the device as it is prone to low-mobility percolation paths with wide-angle grain boundaries.

Morphology Measurements

Figure 12 shows tapping mode AFM images of various thin film compositions being studied. The films of ITIC-Th based blends generally showed a smoother surface with an rms of 2.877 nm and 3.198 nm for P3HT:ITIC-Th and PBDB-T:ITIC-Th, respectively. On the other hand, when the fullerene acceptor was used to make PBDB-T:PC_{71}BM and P3HT:PC_{71}BM, increased rms of 4.146 and 3.301 nm, respectively were recorded (**Figure 12**). Since the AFM images show a topographical image of the height correlations of a 2D surface, it is rather difficult to correlate our rms roughness with the vertical scale morphology as the aspect ratio of the rms roughness to film thickness is very small. The low roughness observed for these blend layers are rather promising owing to the lack of hillock formation which degrades performance.

CONCLUSION

Air processed OSC devices using PBDB-T and P3HT as donor materials blended with either a fullerene derivative (PC_{71}BM) or a non-fullerene derivative (ITIC-Th) have been fabricated and tested with an aim of understanding factors leading to differences in their performances. Generally, the non-fullerene ITIC-Th based blend shows better optical absorption compared to fullerene (PC_{71}BM) based blends with PBDB-T:ITIC-Th recording higher absorption intensity but over a shorter wavelength range compared to P3HT:ITIC-Th which absorbs more to the green side of the spectrum. On the contrary, the fullerene (PC_{71}BM) acceptor-based blends showed higher PL quenching, an indication of better charge transfer. The P3HT:ITIC-Th blend recorded the lowest PCE performance characterized by lowest maximum exciton generation rate (G_{max}) of 0.96×10^{28} s^{-1} and lowest charge dissociation and collection probability P(E,T) of 66.2%. We observed the lowest V_{oc} in the P3HT:ITIC-Th blend occasioned by very strong recombination processes. This is in agreement with the high degree of crystallinity seen from Raman spectra that leads to large phase separation. The PBDB-T:PC_{71}BM blend recorded the best device performance, yielding a saturation photocurrent density (J_{sat}) of 11.08 mA/cm^2 and maximum exciton generation rate (G_{max}) of 3.22×10^{28} s^{-1}, resulting in the highest short circuit density and PCE of 10.22 mA/cm^2 and 4.49%, respectively.

DATA AVAILABILITY STATEMENT

The raw data supporting the conclusions of this article will be made available by the authors, without undue reservation.

AUTHOR CONTRIBUTIONS

FO carried out all the experiments and a part of manuscript preparation. LK designed blend ratios and J–V measurements MA carried out project conceptualization, Raman spectroscopy analysis, and manuscript preparations. RE carried out PL and Raman spectroscopy measurements, analysis, and manuscript review. CB carried out impedance measurements, manuscript writing and revision. DW conceptualized the project and reviewed the manuscript while DB is the postdoc host to FO and funding, aspects of project conceptualization. All authors contributed to the article and approved the submitted version.

ACKNOWLEDGMENTS

The authors would like to thank the Synchrotron Techniques for Africa Research and Technology-Global Challenge Research Fund (START-GCRF) under UKRI (Grant No. ST/R002754/1) for postdoctoral funding, the Molecular Science Institute, School of Chemistry, Material Physics Research Institute, School of Physics, University of the Witwatersrand (posdoc 2018-2021), the MMU facilities at Wits and NRF (South Africa).

SUPPLEMENTARY MATERIAL

The Supplementary Material for this article can be found online at: https://www.frontiersin.org/articles/10.3389/fenrg.2021.640664/full#supplementary-material

REFERENCES

Arulraj, A., Bhuvaneshwari, S., Senguttuvan, G., and Ramesh, M. (2018). Solution processed inverted organic bulk heterojunction solar cells under ambient air-atmosphere. *J. Inorg. Organomet. Polym. Mater.* 28, 1029–1036. doi: 10.1007/s10904-017-0762-y

Chen, J. D., Cui, C., Li, Y. Q., Zhou, L., Ou, Q. D., Li, C., et al. (2015). Single-junction polymer solar cells exceeding 10% power conversion efficiency. *Adv. Mater.* 27, 1035–1041. doi: 10.1002/adma.201404535

Falke, S. M., Rozzi, C. A., Brida, D., Maiuri, M., Amato, M., Sommer, E., et al. (2014). Coherent ultrafast charge transfer in an organic photovoltaic blend. *Science* 344, 1001–1005. doi: 10.1126/science.1249771

Falke, S., Eravuchira, P., Materny, A., and Lienau, C. (2011). Raman spectroscopic identification of fullerene inclusions in polymer/fullerene blends. *J. Raman Spectrosc.* 42, 1897–1900. doi: 10.1002/jrs.2966

Gadisa, A. (2006). *Studies of Charge Transport and Energy Level in Solar Cells Based on Polymer/Fullerene Bulk Heterojunction*. Doctoral thesis. Linköping: Institutionen för Fysik, Kemi och Biologi, Linköping University.

Gao, J., Wang, W., Zhang, S., Xiao, S., Zhan, C., Yang, M., et al. (2018). Distinction between PTB7-Th samples prepared from Pd (PPh 3) 4 and Pd 2 (dba) 3/P (o-tol) 3 catalysed stille coupling polymerization and the resultant photovoltaic performance. *J. Mater. Chem. A* 6, 179–188. doi: 10.1039/c7ta09464g

Gao, Y., Liu, M., Zhang, Y., Liu, Z., Yang, Y., and Zhao, L. (2017). Recent development on narrow bandgap conjugated polymers for polymer solar cells. *Polymers* 9:39. doi: 10.3390/polym9020039

Gélinas, S., Rao, A., Kumar, A., Smith, S. L., Chin, A. W., Clark, J., et al. (2014). Ultrafast long-range charge separation in organic semiconductor photovoltaic diodes. *Science* 343, 512–516. doi: 10.1126/science.1246249

Grey, J. K. (2019). Resonance raman spectroscopy and imaging of franck–condon vibrational activity and morphology in conjugated polymers for solar cells. *Acc. Chem. Res.* 52, 2221–2231. doi: 10.1021/acs.accounts.9b00088

Gurney, R. S., Lidzey, D. G., and Wang, T. (2019). A review of non-fullerene polymer solar cells: from device physics to morphology control. *Rep. Prog. Phys.* 82:036601. doi: 10.1088/1361-6633/ab0530

He, C., Zhong, C., Wu, H., Yang, R., Yang, W., Huang, F., et al. (2010). Origin of the enhanced open-circuit voltage in polymer solar cells via interfacial modification using conjugated polyelectrolytes. *J. Mater. Chem.* 20, 2617–2622. doi: 10.1039/b921775d

Kabongo, G. L., Mbule, P. S., Mhlongo, G. H., Mothudi, B. M., Hillie, K. T., and Dhlamini, M. S. (2016). Photoluminescence quenching and enhanced optical conductivity of P3HT-derived Ho 3+-doped ZnO nanostructures. *Nanoscale Res. Lett.* 11, 1–11.

Kim, Y., Cook, S., Tuladhar, S. M., Choulis, S. A., Nelson, J., Durrant, J. R., et al. (2011). "A strong regioregularity effect in self-organizing conjugated polymer films and high-efficiency polythiophene: fullerene solar cells," in *Materials For Sustainable Energy: A Collection of Peer-Reviewed Research and Review Articles from Nature Publishing Group*, 63–69.

Kroon, R., Lenes, M., Hummelen, J. C., Blom, P. W., and De Boer, B. (2008). Small bandgap polymers for organic solar cells (polymer material development in the last 5 years). *Polym. Rev.* 48, 531–582. doi: 10.1080/15583720802231833

Li, J., Liang, Z., Peng, Y., Lv, J., Ma, X., Wang, Y., et al. (2018). 36% enhanced efficiency of ternary organic solar cells by doping a NT-based polymer as an electron-cascade donor. *Polymers* 10:703. doi: 10.3390/polym10070703

Li, S., Ye, L., Zhao, W., Zhang, S., Mukherjee, S., Ade, H., et al. (2016). Energy-level modulation of small-molecule electron acceptors to achieve over 12% efficiency in polymer solar cells. *Adv. Mater.* 28, 9423–9429. doi: 10.1002/adma.201602776

Lin, Y., and Zhan, X. (2014). Non-fullerene acceptors for organic photovoltaics: an emerging horizon. *Mater. Horiz.* 1, 470–488. doi: 10.1039/c4mh00042k

Lin, Y., Zhao, F., He, Q., Huo, L., Wu, Y., Parker, T. C., et al. (2016). High-performance electron acceptor with thienyl side chains for organic photovoltaics. *J. Am. Chem. Soc.* 138, 4955–4961. doi: 10.1021/jacs.6b02004

Liu, S., You, P., Li, J., Li, J., Lee, C.-S., Ong, B. S., et al. (2015). Enhanced efficiency of polymer solar cells by adding a high-mobility conjugated polymer. *Energy Environ. Sci.* 8, 1463–1470. doi: 10.1039/c5ee00090d

Liu, T., Meng, D., Cai, Y., Sun, X., Li, Y., Huo, L., et al. (2016). High-performance non-fullerene organic solar cells based on a selenium-containing polymer donor and a twisted perylene bisimide acceptor. *Adv. Sci.* 3:1600117. doi: 10.1002/advs.201600117

Lu, L., Chen, W., Xu, T., and Yu, L. (2015). High-performance ternary blend polymer solar cells involving both energy transfer and hole relay processes. *Nat. Commun.* 6:7327.

Martens, H., Blom, P., and Schoo, H. (2000). Comparative study of hole transport in poly (p-phenylene vinylene) derivatives. *Phys. Rev. B* 61:7489. doi: 10.1103/physrevb.61.7489

Motaung, D. E., Malgas, G. F., Arendse, C. J., Mavundla, S. E., Oliphant, C. J., and Knoesen, D. (2009). Thermal-induced changes on the properties of spin-coated P3HT: C60 thin films for solar cell applications. *Sol. Energy Mater. Sol. Cells* 93, 1674–1680. doi: 10.1016/j.solmat.2009.05.016

Nicho, M., Hu, H., ópez-Mata, C. L., and Escalante, J. (2004). Synthesis of derivatives of polythiophene and their application in an electrochromic device. *Sol. Energy Mater. Sol. Cells* 82, 105–118. doi: 10.1016/j.solmat.2004.01.009

Otieno, F., Airo, M., Ranganathan, K., and Wamwangi, D. (2016). Annealed silver-islands for enhanced optical absorption in organic solar cell. *Thin Solid Films* 598, 177–183. doi: 10.1016/j.tsf.2015.11.076

Otieno, F., Mutuma, B. K., Airo, M., Ranganathan, K., Erasmus, R., Coville, N., et al. (2017). Enhancement of organic photovoltaic device performance via P3HT: PCBM solution heat treatment. *Thin Solid Films* 625, 62–69.

Qian, D., Ye, L., Zhang, M., Liang, Y., Li, L., Huang, Y., et al. (2012). Design, application, and morphology study of a new photovoltaic polymer with strong aggregation in solution state. *Macromolecules* 45, 9611–9617.

Qin, Y., Uddin, M. A., Chen, Y., Jang, B., Zhao, K., Zheng, Z., et al. (2016). Highly efficient fullerene-free polymer solar cells fabricated with polythiophene derivative. *Adv. Mater.* 28, 9416–9422. doi: 10.1002/adma.201601803

Riedel, I., Parisi, J., Dyakonov, V., Lutsen, L., Vanderzande, D., and Hummelen, J. C. (2004). Effect of temperature and illumination on the electrical characteristics of polymer–fullerene bulk-heterojunction solar cells. *Adv. Funct. Mater.* 14, 38–44. doi: 10.1002/adfm.200304399

Roigé, A., Campoy-Quiles, M., Ossó, J., Alonso, M., Vega, L., and Garriga, M. (2012). Surface vs bulk phase transitions in semiconducting polymer films for OPV and OLED applications. *Synth. Met.* 161, 2570–2574. doi: 10.1016/j.synthmet.2011.09.031

San Juan, R. R., Payne, A.-J., Welch, G. C., and Ala'a, F. E. (2016). Development of low band gap molecular donors with phthalimide terminal groups for use in solution processed organic solar cells. *Dyes Pigm.* 132, 369–377. doi: 10.1016/j.dyepig.2016.05.015

Servaites, J. D., Ratner, M. A., and Marks, T. J. (2011). Organic solar cells: a new look at traditional models. *Energy Environ. Sci.* 4, 4410–4422.

Smestad, G. P., Krebs, F. C., Lampert, C. M., Granqvist, C. G., Chopra, K., Mathew, X., et al. (2008). Reporting solar cell efficiencies in solar energy materials and solar cells. *Sol. Energy Mater. Sol. Cells* 92, 371–373. doi: 10.1016/j.solmat.2008.01.003

Street, R., Northrup, J., and Salleo, A. (2005). Transport in polycrystalline polymer thin-film transistors. *Phys. Rev. B* 71:165202.

Suprunov, V., and Ivanov, A. (1987). Adsorption forms of phenol on Cr 2 O 3 and their reactivity. *React. Kinet. Catal. Lett.* 33, 75–80. doi: 10.1007/bf02066703

Tsoi, W. C., James, D. T., Kim, J. S., Nicholson, P. G., Murphy, C. E., Bradley, D. D., et al. (2011). The nature of in-plane skeleton Raman modes of P3HT and their correlation to the degree of molecular order in P3HT: PCBM blend thin films. *J. Am. Chem. Soc.* 133, 9834–9843. doi: 10.1021/ja2013104

Xiao, L., He, B., Hu, Q., Maserati, L., Zhao, Y., Yang, B., et al. (2018). Multiple roles of a non-fullerene acceptor contribute synergistically for high-efficiency ternary organic photovoltaics. *Joule* 2, 2154–2166. doi: 10.1016/j.joule.2018.08.002

Yang, G., Wang, Z., Duan, Y., Zhao, D., and Yu, J. (2019). High-performance organic photodetectors by introducing a non-fullerene acceptor to broaden long wavelength detective spectrum. *Nano. Res. Lett.* 14:201.

Zakhidov, E., Zakhidova, M., Imomov, M. K., Kuvondikov, V., Nematov, S. K., and Saparbaev, A. I (2020). Tazhibaev, correlation of degradation of P3HT: PCBM and P3HT: ITIC organic solar cells with changes of their optical spectra. *J. Appl. Spectrosc.* 87, 464–470.

Zhang, Y., Li, X., Dai, T., Ha, W., Du, H., Li, S., et al. (2019). Charge transport and extraction of bilayer interdiffusion heterojunction organic solar cells. *J. Phys. Chem. C* 123, 24446–24452. doi: 10.1021/acs.jpcc.9b08242

Zhao, J., Li, Y., Lin, H., Liu, Y., Jiang, K., Mu, C., et al. (2015). High-efficiency non-fullerene organic solar cells enabled by a difluorobenzothiadiazole-based donor

polymer combined with a properly matched small molecule acceptor. *Energy Environ. Sci.* 8, 520–525. doi: 10.1039/c4ee02990a

Zhao, W., Li, S., Zhang, S., Liu, X., and Hou, J. (2017). Ternary polymer solar cells based on two acceptors and one donor for achieving 12.2% efficiency. *Adv. Mater.* 29:1604059. doi: 10.1002/adma.201604059

Zhao, W., Ye, L., Zhang, S., Sun, M., and Hou, J. (2015). A universal halogen-free solvent system for highly efficient polymer solar cells. *J. Mater. Chem. A* 3, 12723–12729.

Zhou, Y., Fuentes-Hernandez, C., Shim, J., Meyer, J., Giordano, A. J., Li, H., et al. (2012). A universal method to produce low–work function electrodes for organic electronics. *Science* 336, 327–332.

Conflict of Interest: The authors declare that the research was conducted in the absence of any commercial or financial relationships that could be construed as a potential conflict of interest.